Review Article

Xiehui Li, Hejia Jia, Lei Wang*, and Tiangui Xiao

Prediction and assessment of meteorological drought in southwest China using long short-term memory model

https://doi.org/10.1515/geo-2022-0708
received February 14, 2024; accepted September 18, 2024

Abstract: Drought prediction is crucial for mitigating risks and designing measures to alleviate its impact. Machine learning models have been widely applied in the field of drought prediction in recent years. This study concentrated on predicting meteorological droughts in southwest China, a region prone to frequent and severe droughts, particularly in areas with sparse meteorological station coverage. The long short-term memory (LSTM) predictive model, which is a deep learning model, was constructed by calculating standardized precipitation evapotranspiration index (SPEI) values based on 144 weather station observations from 1980 to 2020. The 5-fold cross-validation method was used for the hyperparameter optimization of the model. The LSTM model underwent comprehensive assessment and validation through multiple methods. This included the use of several accuracy assessment indicators and a comparison of results. The comparison covered different drought characteristics among the LSTM predictive model, the benchmark random forest (RF) predictive model, the historical drought situations, and the calculated SPEI values based on observations from 144 weather stations. The results showed that the training results of the LSTM predictive model basically agreed with the SPEI values calculated from weather station observations. The model-predicted variation trend of SPEI values for 2020 was similar to the variation in SPEI values calculated based on weather station observations. On the test set, the coefficient of determination (R^2), the root mean square error, the explained variance score, the Nash–Sutcliffe efficiency, and the Kling–Gupta efficiency were 0.757, 0.210, 0.802, 0.761, and 0.212, respectively. The total consistency rate of the drought grade was 59.26%. The spatial correlation distribution of SPEI values between LSTM model prediction and calculation from meteorological stations in 2020 was more than 0.5 for most regions. The correlation coefficients exceeded 0.6 in western Tibet and Chengdu Plains. Compared to the RF model, the LSTM model excelled in all five performance evaluation metrics and demonstrated a higher overall consistency rate for drought categories. The Kruskal–Wallis test for both the LSTM and RF models all indicated no significant difference in the distributions between the predicted and observed data. Scatter plots revealed that the prediction accuracy for both models in 2020 was suboptimal, with the SPEI showing a comparatively narrow range of values. Nonetheless, the LSTM model significantly outperformed the RF model in terms of prediction accuracy. In summary, the LSTM model demonstrated good overall performance, accuracy, and applicability. It has the potential to enhance dynamic drought prediction in regions with complex terrain, diverse climatic factors, and sparse weather station networks.

Keywords: drought prediction, drought assessment, SPEI, LSTM model, RF model, southwest China

*** Corresponding author: Lei Wang,** School of Atmospheric Sciences, Chengdu University of Information Technology, Chengdu, 610225, Sichuan, China, e-mail: lwang@cuit.edu.cn
Xiehui Li: School of Atmospheric Sciences, Chengdu University of Information Technology, Chengdu, 610225, Sichuan, China; Yunnan R&D Institute of Natural Disaster on Chengdu University of Information Technology, Kunming, 650034, Yunnan, China; Key Open Laboratory of Arid Climate Change and Disaster Reducing, China Meteorological Administration, Lanzhou, 730020, Gansu, China
Hejia Jia: School of Atmospheric Sciences, Chengdu University of Information Technology, Chengdu, 610225, Sichuan, China; Xianning Meteorological Service, Xianning, 437000, Hubei, China
Tiangui Xiao: School of Atmospheric Sciences, Chengdu University of Information Technology, Chengdu, 610225, Sichuan, China; Yunnan R&D Institute of Natural Disaster on Chengdu University of Information Technology, Kunming, 650034, Yunnan, China

1 Introduction

Drought usually originates from precipitation deficits and propagates through the hydrological cycle [1]. Few natural hazards are as devastating as drought worldwide, which is an unavoidable recurrent occurrence, affecting more than

half of the world every year [2,3]. According to the Drought in Numbers 2022 Report released by the United Nations Convention to Combat Desertification, the frequency and duration of droughts have increased by 29% since 2000 and will increase in the next few decades in 129 countries worldwide. Approximately 650,000 people died from drought between 1970 and 2019. From 1998 to 2017, drought caused economic losses of approximately $124 billion globally. In 2022, more than 2.3 billion people faced water resource pressure, and nearly 160 million children suffered from severe and long-term drought. If the increase in global warming relative to pre-industrial temperature levels reaches 3°C by 2100, drought losses may be five times higher than they are now. If no action is taken, an estimated 700 million people will face the risk of displacement due to drought by 2030. One in every four children is estimated to live in areas with extreme water scarcity by 2040. Also, by 2050, drought may affect more than three-quarters of the world's population, with an estimated 4.8–5.7 billion people facing water scarcity for at least 1 month each year (currently 3.6 billion people) [4,5]. Therefore, accurately predicting drought events and their spatiotemporal patterns is paramount for taking proactive measures and minimizing adverse impacts [6].

Defining the natural phenomena of drought is complex owing to its region-specific nature. However, precipitation deficit can be considered as the root cause of drought [7]. Generally, drought is classified into four categories based on its impact: meteorological drought, agriculture drought, hydrological drought, and socioeconomic drought. Among these, meteorological drought is the basis of the other three types of drought. As drought indices offer a quantitative description of the duration, severity, and extent of drought, they constitute the foundation for modern drought predictive modeling. Different drought types have different drought indices [5]. More than a hundred drought indices have been developed so far, including (but not limited to) the well-known meteorological drought indices such as the Palmer drought index (PDSI), the drought area index, the standardized precipitation index (SPI), standardized precipitation evapotranspiration index (SPEI), and the reconnaissance drought index [3,8]. Among these, as the name implies, SPEI considers the effects of both evaporation and precipitation values on drought severity, which builds on the algorithms used in both SPI and PDSI. SPEI can identify different drought types under the background of global warming and is widely used to analyze, monitor, and predict drought. It can also measure drought severity according to intensity and duration and identify the beginning and end of drought events [3,9]. Therefore, this study selected SPEI to analyze drought characteristics.

Drought has multivariate, nonlinear, and stochastic characteristics [10]. Various approaches are used for drought prediction. Among these, statistical, dynamical, and hybrid models are prominent. The commonly used statistical models are implemented using various algorithms such as Markov chain, fuzzy logic, classification and regression algorithms of machine learning (ML), and deep learning (DL) algorithms; different hybrid algorithms are also used [7,11]. ML has developed exponentially in recent years in the field of artificial intelligence. An increasing number of researchers have used different ML algorithms to predict drought from different timescales in various parts of the world [12]. The ML algorithms used include the *k*-nearest neighbor, random forest (RF), support vector machine, decision tree, multivariate adaptive regression spline (MARS), *k* means, boosted regression tree, classification and regression tree, eXtreme gradient boosting, Cubist, extreme learning machine, multilayer perceptron, and autoregressive integrated moving average (ARIMA) [12–22].

With the advent of the Big Data era, researchers are challenged by the problems of complex data structure, massive data volume, and variable data quality. Conventional ML methods require the use of a large amount of professional knowledge in the target areas to do the modeling. That is, the researchers should know enough about the model and take a lot of time in manually designing a feature extractor for converting raw data into an appropriate internal representation. For this reason, conventional ML methods are inadequate for building drought prediction models, whereas artificial neural network (ANN) offers promising solutions. Especially, Hinton and Salakhutdinov [23] proposed DL based on a deep neural network (DNN) in 2006, which combined several layers of nonlinear modules for feature conversion. DL can automatically perform feature extraction from massive amounts of data and learn multilayer feature representation. Its nonlinear multilayer architecture makes it possible to model complex tasks. For time-series prediction tasks, DL can effectively extract features from time series and achieve high predictive performance. This method is suitable for drought prediction based on nonlinear and nonstationary time series [3,24,25]. Main DL algorithms include DNN, convolutional neural network, recurrent neural network (RNN), and generative adversarial network.

The DL methods can not only extract more useful features from a large number of drought factors but also excel in handling nonlinear and nonstationary relationships between input features, thereby improving the prediction ability of drought. They can have great potential beyond previous modeling methods. Long short-term memory (LSTM) is recognized as an advanced form of RNN, which can cover the flaws of general RNN structure through long-term dependency learning [26]. Some researchers attempted to use the

LSTM model to predict drought. An increase in drought prediction accuracy is usually achieved compared with conventional ML and shallow learning, with a prolongation of forecast lead time. Poornima and Pushpalatha [27] compared the 1-, 6-, and 12-month prediction of the ARIMA statistical model with LSTM using multivariate input, hoping to improve said performance. The conclusions showed that the LSTM model provided better results than the ARIMA model for predictions on a longer timescale. Zhang et al. [28] proposed an LSTM method to predict the historical monthly soil moisture time-series data from 1980 to 2012. Comparing the performance of the proposed LSTM model with the ARIMA and autoregressive model, the results demonstrated that the proposed LSTM method (0.0088) had much lower root mean square error (RMSE) than the ARIMA (0.0950) and AR (0.0246) models. Dikshit et al. [29] used the LSTM method to predict the SPEI at 1-month (SPEI-1) and 3-month (SPEI-3) timescale. A comparison of the LSTM model with RF and ANN revealed that the former achieved an R^2 value of more than 0.99 for both SPEI-1 and SPEI-3 cases. Also, the LSTM model showed an improvement relative to ML models for a lead time of 1 month in terms of different drought characteristics. Firdaus et al. [7] took the Latur region of Maharashtra in India as an example for predicting drought indices at varying timescales using SVR and LSTM models. The results showed that the LSTM model outperformed for all three indices SPI, SPEI, and RDI compared with the SVR model. Docheshmeh et al. (2022) [28] investigated the capability of an LSTM model in predicting drought calculated from monthly rainfall data obtained from four stations of Iran. The LSTM method performed superior to the extra-trees, vector autoregressive approach (VAR), and MARS in predicting drought based on different timescales of SPI. The evaluation outcomes recommended using the LSTM model in predicting SPI-based droughts. Wang et al. [30] proposed a drought prediction and evaluation framework based on the LSTM model. A scheme directly used ten diverse factors and historical SPEI to predict future SPEI, further assessing future drought characteristics. The results indicated that the LSTM model significantly improved accuracy when handling high-dimensional complex data and predicting key factors such as precipitation, evaporation, and temperature. The average error of drought severity for light, moderate, severe, and extreme drought levels was 0.05, 0.25, 0.64, and 1.48, respectively. Villegas-Ch and García-Ortiz [31] constructed and evaluated a drought prediction model using the LSTM model based on historical information from local meteorological stations. The results demonstrated that the proposed LSTM model achieved a remarkable accuracy of 98.5% and a high sensitivity of 97.2% in predicting drought events in the coastal region of Ecuador. Based on these existing research results, this study chose the LSTM model to predict the drought characteristics in southwest China.

Southwest China is a vast region that is highly vulnerable to drought, influenced by water vapor from the Bay of Bengal and the south trough. This area is characterized by its diverse terrain and topography, encompassing the Qinghai–Tibet Plateau, the Yunnan–Guizhou Plateau, the Hengduan Mountain Range, and the Sichuan Basin. Historically, southwest China has experienced frequent severe and intense droughts [32]. The factors contributing to drought and the mechanisms behind it vary significantly within this region [32–35]. Establishing weather stations is particularly challenging in the high-altitude areas of the Qinghai–Tibet Plateau and the Yunnan–Guizhou Plateau. The limited number of weather stations in these regions exacerbates the shortage of meteorological data. Additionally, global warming has led to an increase in both the frequency and intensity of drought events [36]. Consequently, there is an urgent need for a precise and adaptive drought prediction model to mitigate the impacts in southwest China. DL methods are currently less used for drought prediction in southwest China. Therefore, the present study mainly completed the following tasks: (1) SPEI values were calculated based on 144 weather station observations from 1980 to 2020 in southwest China; (2) an LSTM prediction model was constructed based on monthly SPEI values from 1980 to 2019, and SPEI values were predicted in 2020; (3) the performance of the LSTM model was comprehensively assessed and validated by not only using several accuracy assessment indicators but also comparing the results on different drought characteristics (the spatial and temporal distributions, grades, and scope of impact) among the LSTM model, the historical drought situations, and the calculated SPEI values from 144 weather station observations; and (4) a benchmark RF model was also developed, and a comprehensive comparative analysis of its predictive performance was carried out in comparison with the LSTM model. The research aimed to develop a DL LSTM model designed to manage long-term dependencies effectively, model nonlinear relationships, automatically extract key features from data, adapt flexibly, require minimal computational resources, reduce overfitting risk, and ensure high accuracy. The purpose was to improve the level of dynamic drought prediction in regions characterized by complex terrain and topography and formative factors of weather and climate and where weather stations were sparsely distributed. By accurately and timely predicting drought, decision-makers can take appropriate measures to mitigate the adverse effects of drought on society, economy, and environment, and ensure the achievement of sustainable development and resource utilization goals in southwest China [6].

2 Data and methods

2.1 Study area

Southwest China extends longitudinally from 78°42′E to 110°11′E and latitudinally from 21°13′N to 36°53′N. It shares borders with India, Laos, Bhutan, Nepal, Pakistan, and Myanmar, covering an area of 2.34 million km², which represents about 24.5% of China's total land area [37]. This region includes five provinces and municipalities: Yunnan, Sichuan, Chongqing, Guizhou, and Tibet. It features a mix of subtropical monsoon and alpine climates, with annual precipitation ranging from 600 to 2,300 mm and average temperatures varying between −2.8 and 23.9°C. Rainfall is unevenly distributed, with the eastern areas experiencing much higher precipitation compared to the western regions, where the disparity can reach up to five-fold between the wettest and driest locations [38,39]. Given the region's complex geography and climate, agricultural development exhibits a range of characteristics. Key staple crops include rice, corn, wheat, potatoes, and soybeans. Additionally, there has been substantial development in horticultural crops and traditional Chinese medicinal herbs. Southwest China is also a significant base for tobacco, tea, and fruit production. Consequently, droughts can lead to considerable losses in agricultural productivity across these various sectors.

2.2 Data

The daily meteorological observations included the temperature and precipitation data from 144 weather stations in southwest China from 1980 to 2020, which were downloaded from data.cma.cn. The data of weather stations underwent three preprocessing steps to ensure quality control: checks for internal consistency, assessments of climatic threshold values, and evaluations of extreme station values [40]. To handle the limited missing data from 144 weather stations, interpolation was conducted by utilizing average values of the same meteorological element from corresponding days across different years. These methods were employed to improve the accuracy and scientific validity of the meteorological observations. The drought disaster data for southwest China in 2020 were sourced from the 2020 China Climate Bulletin [41]. Figure 1 illustrates the geographic location of the study area and the spatial distributions of elevation and weather stations [32].

2.3 Methods

2.3.1 Calculation of SPEI

Vicente-Serrano et al. [42] first proposed the SPEI based on SPI considering both water deficit and cumulative effects. SPEI is an index obtained by calculating the difference between precipitation and potential evapotranspiration (PET) [43]. Some methods used to calculate PET include the Penman–Monteith method recommended by the Food and Agriculture Organization of the United Nations as the standard method for calculating evapotranspiration with high accuracy. However, its disadvantage is that it requires many meteorological parameters, which is not easy to obtain in many parts of the world [9]. PET can also be calculated using the Thornthwaite method to obey a log-logistic probability distribution, which requires few meteorological elements [43]. In the present study, we used the Thornthwaite method to calculate PET. SPEI was calculated using the following formula, where the monthly climatic water balance D_i of month i was initially computed using

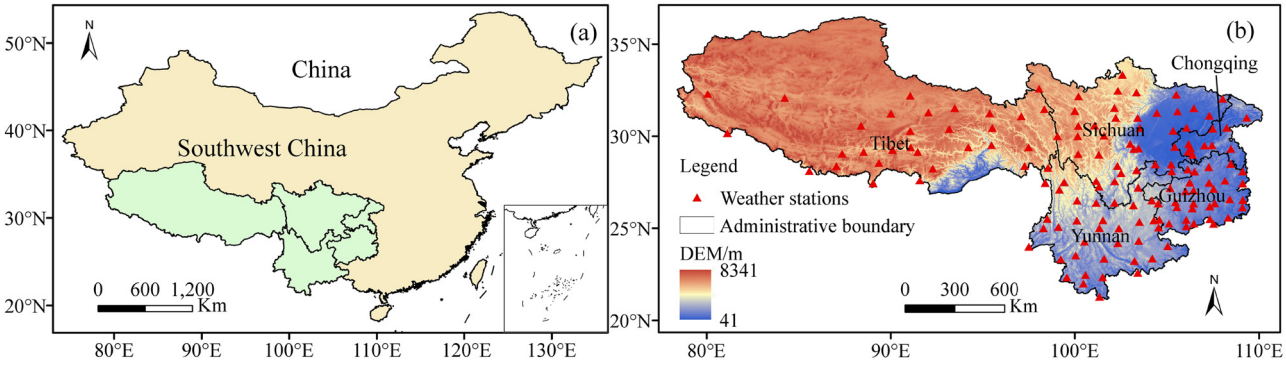

Figure 1: Geographical location (a) and spatial distribution of DEM and weather stations (b) in southwest China.

the difference between precipitation P_i and PET_i and was expressed as follows [27,42,44]:

$$D_i = P_i - \mathrm{PET}_i. \tag{1}$$

The calculated D_i values were aggregated at different timescales. SPEI was calculated using the three-parameter log-logistic distribution based on the standardized D series. The probability distribution function $F(x)$ of the log-logistic distribution for the D series was expressed as

$$F(x) = \left[1 + \left(\frac{\alpha}{x - \gamma}\right)^{\beta}\right]^{-1}, \tag{2}$$

where α, β, and γ are the scale, shape, and origin parameters, respectively, which were obtained using the L-moment procedure [42]:

$$\alpha = \frac{(W_0 - 2W_1)\beta}{\Gamma(1 + 1/\beta)\Gamma(1 - 1/\beta)}, \tag{3}$$

$$\beta = \frac{(2W_1 - W_0)}{(6W_1 - W_0 - 6W_2)}, \tag{4}$$

$$\gamma = W_0 - \alpha\Gamma(1 + 1/\beta)\Gamma(1 - 1/\beta), \tag{5}$$

where $\Gamma(1 + 1/\beta)$ is the gamma function of $(1 + 1/\beta)$, and W_s is the probability-weighted moment of order s (s = 0, 1, 2), which was calculated as follows:

$$W_s = \frac{1}{N}\sum_{i=1}^{N}\left(1 - \frac{i - 0.35}{N}\right)^{s} D_i, \tag{6}$$

where N is the number of data points and i is the range of observations in increasing order. SPEI was then calculated as the standardized values of $F(x)$, as follows:

$$P = 1 - F(x), \tag{7}$$

When $P \le 0.5$,

$$\mathrm{SPEI} = W - \frac{C_0 - C_1W + C_2W^2}{1 + d_1W + d_2w^2 + d_3w^3}. \tag{8}$$

When $P > 0.5$, the value of P is $1 - P$,

$$\mathrm{SPEI} = -\left(W - \frac{C_0 - C_1W + C_2W^2}{1 + d_1W + d_2w^2 + d_3w^3}\right), \tag{9}$$

Table 1: Drought classification based on SPEI value [32,44–48]

Level	Classification	SPEI threshold
1	No drought	−0.5 < SPEI
2	Mild drought	−1.0 < SPEI ≦ −0.5
3	Moderate drought	−1.5 < SPEI ≦ −1.0
4	Severe drought	−2.0 < SPEI ≦ −1.5
5	Extreme drought	SPEI ≤ −2.0

$$W = \sqrt{-2\ln(P)}, \tag{10}$$

where P is the cumulative probability, W is the weighted moment of cumulative probability, and the constant values are c_0 = 2.515517, c_1 = 0.802853, c_2 = 0.010328, d_1 = 1.432788, d_2 = 0.189269, and d_3 = 0.001308. The drought categories classified according to the SPEI values are shown in Table 1.

2.3.2 LSTM model

Hochreiter and Schmidhuber proposed LSTM for the first time in 1997 [49] to solve the problem of blowing up or decaying error backflow in original RNNs. However, this model has been improved and generalized progressively by numerous scholars. The LSTM model is one of the DL techniques showing a great ability for dealing with time-series problems by considering information selections and long-term dependencies [50]. It incorporates several recurrently connected blocks to control the memory of each neural layer. These memory blocks include three main units: input, output, and forget gates [51]. The gates are considered multiplicative units and can be activated or closed to control the error flow. Hence, LSTM can effectively capture the long-term temporal dependencies, without suffering many optimization hurdles. A schematic of a typical LSTM memory block is shown in Figure 2, and detailed equations of each component are explained in equations (11)–(16) [52].

$$f_t = \sigma(W_\mathrm{f} \cdot [h_{t-1}, x_t] + b_\mathrm{f}), \tag{11}$$

$$i_t = \sigma(W_\mathrm{i} \cdot [h_{t-1}, x_t] + b_\mathrm{i}), \tag{12}$$

$$\tilde{C}_t = \tanh(W_\mathrm{c} \cdot [h_{t-1}, x_t] + b_\mathrm{c}), \tag{13}$$

$$C_t = f_t \times C_{t-1} + i_t \times \tilde{C}_t, \tag{14}$$

$$o_t = \sigma(W_\mathrm{o} \cdot [h_{t-1}, x_t] + b_\mathrm{o}), \tag{15}$$

$$h_t = o_t \times \tanh(C_t), \tag{16}$$

where x_t is the input vector at time t with σ being the activation function such as sigmoid or rectified linear unit. W_f, W_i, W_c, and W_o are the applied weights to concatenate the new input x_t and output h_{t-1} from the previous cell, with b_f, b_i, b_c, and b_o being the corresponding bias. f_t, i_t, and o_t are the outputs of the three sigmoid functions σ, and the values range from 0 to 1. These control the information forgotten in the old cell state C_{t-1} and passed to the new cell C_t with the new information being $\tilde{C}_t$, where h_t is the output information from the cell [37]. The first step in LSTM is deciding what information from the input x_t is going to be removed from the cell state h_{t-1} by forget gate f_t. The next step is to decide what new information

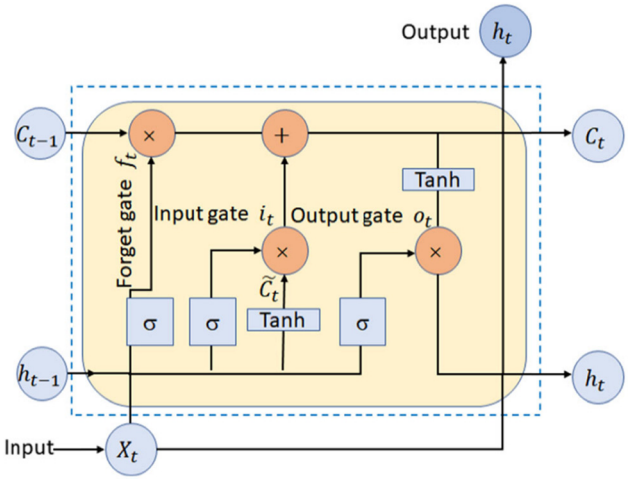

Figure 2: Structure of the LSTM model [52].

is stored in the cell state. It includes the sigmoid layer as an input gate to decide values to be updated, and the tanh layer creates a new candidate value ($\widetilde{C}_t$) that can be added to the state. The old cell state (C_{t-1}) is updated to the new cell state C_t. The output h_t is addressed by the sigmoid layer to decide what part of the cell state will go to the output o_t, and the cell state updates output through the tanh layer.

Due to the LSTM model's advantages, including its ability to effectively capture long-term dependencies in time series, model nonlinear relationships, automatically extract significant features from data, demonstrate high flexibility, and integrate with other models, it has made notable progress in areas such as drought prediction. Nevertheless, several limitations must be addressed, including high data requirements, extended training times, the risk of overfitting, poor interpretability, and challenges in handling very long time-series data. These factors should be carefully considered when applying the model.

2.3.3 Benchmark model-RF

The RF method, introduced by Breiman in 2001, is a robust and versatile ML algorithm extensively used for both classification and regression tasks. RF enhances prediction accuracy and mitigates overfitting by aggregating multiple decision trees. Its strengths include the capacity to handle high-dimensional data, assess feature importance, support parallelization, reduce bias and variance, and maintain robustness to missing data. However, RF also presents certain limitations, such as high computational resource demands, limited model interpretability, significant spatial complexity, longer prediction times, sensitivity to noisy data, and the complexity of parameter tuning [32,53,54]. This study utilized RF as a benchmark model to compare and evaluate the prediction performance of LSTM model.

Classification outcomes are determined through voting among the base classifiers. The final classification result is derived by aggregating the decisions of each decision tree using a majority voting approach. This can be mathematically represented as follows [54]:

$$H(x) = \text{argmax}_Y \sum_{i=1}^{k} I(h_i(x) = Y), \tag{17}$$

where $H(x)$ denotes the final classification result from RF, $h_i(x)$ represents the classification outcome of ith classification and regression tree, Y is the output variable, and $I(\cdot)$ is the indicator function.

2.3.4 Indicators of model accuracy assessment

The accuracy of the prediction model was evaluated by computing and comparing statistical measures based on the differences between the true (observed) and predicted drought index (SPEI): the R^2, explained variance score (EVS), RMSE, Nash–Sutcliffe efficiency (NSE), Kling–Gupta efficiency (KGE), and correlation coefficient (CC) were calculated using equations (18)–(24), respectively [32,45,55,56]:

$$R^2 = 1 - \left[\frac{\sum_{i=1}^{N}(\text{SPEI}_{\text{cal},i} - \text{SPEI}_{\text{pre},i})^2}{\sum_{i=1}^{N}(\text{SPEI}_{\text{pre},i} - \overline{\text{SPEI}}_{\text{pre}})^2}\right], \tag{18}$$

$$\text{EVS} = 1 - \frac{\text{Var}(\text{SPEI}_{\text{cal},i} - \text{SPEI}_{\text{pre},i})}{\text{Var}(\text{SPEI}_{\text{pre},i})}, \tag{19}$$

$$\text{RMSE} = \sqrt{\frac{1}{N}\sum_{i=1}^{N}(\text{SPEI}_{\text{cal},i} - \text{SPEI}_{\text{pre},i})^2}, \tag{20}$$

$$\text{NSE} = 1 - \left[\frac{\sum_{i=1}^{N}(\text{SPEI}_{\text{cal},i} - \text{SPEI}_{\text{pre},i})^2}{\sum_{i=1}^{N}(\text{SPEI}_{\text{cal,i}} - \overline{\text{SPEI}}_{\text{cal}})^2}\right], \tag{21}$$

$$\text{KGE} = 1 - \sqrt{(\text{CC} - 1)^2 + (\beta - 1)^2 + (\gamma - 1)^2}, \tag{22}$$

$$\beta = \frac{\overline{\text{SPEI}}_{\text{pre}}}{\overline{\text{SPEI}}_{\text{cal}}}, \gamma = \frac{\frac{\sigma_{\text{pre},i}}{\text{SPEI}_{\text{pre}}}}{\frac{\sigma_{\text{cal},i}}{\overline{\text{SPEI}}_{\text{cal}}}}, \tag{23}$$

$$\text{CC} = \frac{\sum_{i=1}^{N}(\text{SPEI}_{\text{cal},i} - \overline{\text{SPEI}}_{\text{cal}})\cdot(\text{SPEI}_{\text{pre},i} - \overline{\text{SPEI}}_{\text{pre}})}{\sqrt{\sum_{i=1}^{N}(\text{SPEI}_{\text{cal,i}} - \overline{\text{SPEI}}_{\text{cal}})^2 \cdot \sum_{i=1}^{N}(\text{SPEI}_{\text{pre,i}} - \overline{\text{SPEI}}_{\text{pre}})^2}}, \tag{24}$$

where i represents the data for the ith sample point, N denotes the number of samples, and Var stands for the sample variance. SPEI_{cal} refers to the true SPEI values obtained from weather station observations for the

sample, while $SPEI_{pre}$ denotes the predicted SPEI values for the sample. Additionally, $\overline{SPEI}_{cal}$ and $\overline{SPEI}_{pre}$ represent the average values of the true SPEI values and the predicted SPEI values, respectively. β represents the ratio of the mean of the predicted values to the mean of the observed values, while γ denotes the ratio of the coefficient of variation between the predicted and observed values. The standard deviations of the predicted and observed values are denoted as $\sigma_{pre,i}$ and $\sigma_{cal,i}$, respectively. Among the four indicators, R^2 is a crucial statistic that measures the goodness of fit of the model. EVS is derived from the variance of the error and is used to assess the prediction accuracy of the model. Both R^2 and EVS range from 0 to 1, with values closer to 1 indicating a better model performance. Conversely, the RMSE quantifies the deviation between predicted SPEI values and true SPEI values. RMSE ranges from 0 to ∞, with values nearer to 0 signifying better model accuracy. The NSE is a statistical metric used to evaluate the predictive performance of models by comparing predicted values to observed values. The NSE ranges from −∞ to 1, with a value of 1 indicating perfect predictive accuracy. An NSE value less than 1 is considered ideal, denoting a 100% success rate. Specifically, low predictive success is indicated by an NSE value between 0.3 and 0.5, acceptable predictive success by an NSE value between 0.5 and 0.7, great predictive success by an NSE value between 0.7 and 0.9, and outstanding predictive success by an NSE value between 0.9 and 1 [57–59]. The KGE metric, developed by Kling and Gupta in 2009, improves upon traditional evaluation metrics by incorporating three measures: the CC, the bias ratio (β), and the variability ratio (γ). This combination provides a comprehensive assessment of model performance. Similar to the NSE, the KGE ranges from −∞ to 1, with 1 indicating a perfect match between observed and predicted values [55]. The CC is used to measure the correlation between the two variables. The value of CC is between −1 and 1, the closer its value is to 1 or −1, the stronger the relationship between the true SPEI value and the predicted SPEI value [60,61].

Additionally, for classification problems, the consistency rate was also employed to assess model accuracy. The consistency rate is defined as the ratio of the number of correctly classified samples (where the drought levels of SPEI predicted by the model match those calculated from weather stations) to the total number of samples for a given dataset. This measure reflects how well the model's predictions align with the actual drought levels. The calculation formula is as follows [62,63]:

$$\text{Consistency rate} = C/T, \tag{25}$$

where C is the number of correctly classified samples, and T is the total number of samples.

3 Results and analysis

3.1 Construction of LSTM model

At present, correct drought prediction for Tibet (sparse weather stations) in southwest China still remains a challenge. In our previous study, we compared the applicability of SPEI and meteorological drought composite index (MCI) for drought monitoring in southwest China and demonstrated a higher monitoring performance of SPEI for Tibet than MCI [32,64,65]. The MCI, developed by the National Climate Center by integrating several drought indices, has already been used in China's meteorological businesses. So, this study used the SPEI values calculated from weather station observations in southwest China from 1980 to 2019 as input parameters to construct an LSTM model in Python. The total sample is 480 monthly SPEI values of 144 meteorological stations. The training set was generated by randomly selecting two-thirds of the total sample, and the remaining one-third of the sample constituted the test set. The optimal model was built based on the aforementioned dataset division. Droughts were predicted for the year 2020 based on the SPEI values. The LSTM model obtained was then subjected to parameter tuning by the method of 5-fold cross-validation to determine the optimal parameters in the training set, as shown in Table 2. Here, lr was the learning rate, a parameter that controlled the speed at which the model learned. If lr was too small, the model converged too slowly; if lr was too large, the model might not converge at all. In this study, lr was set to 0.008 to ensure normal convergence. Epoch is the number of iterations for training the ML model with all the training data in one cycle, with the best loss. A nonzero dropout indicates the addition of a dropout layer following any other layers except for the last LSTM layer. The

Table 2: Optimal parameters of the LSTM prediction model

Parameters	Meaning	Optimal parameters
lr	Learning rate	0.008
Epoch	Iterations	600
Dropout	Forgetting layer	0.8
Input_size	Number of input features	1
Output_size	Number of output features	1

corresponding dropout probability is represented by dropout, with a default value of 0. It was set to 0.8 in this study to prevent overfitting. The Input_size represents the number of expected features in the input. As SPEI values were predicted in a one-to-one manner, only one feature was present in the input. Similarly, the output_size represented the number of expected features in the output, and an SPEI value for the year 2020 was the output for each input of the SPEI value. Namely, a single-layer LSTM and a single-feature vector SPEI were mainly used, and the final prediction time step was 12 months by setting a time-slip step to predict the next data with every four-sample input, and eight samples were trained at the same time each time.

Figure 3 shows the temporal variations in the SPEI values obtained by training the LSTM model from 1980 to 2019 and the predicted SPEI values for 2020. The cyan line (true values) represents the SPEI values calculated based on 144 weather station observations in southwest China from 1980 to 2019. The blue line (training predictive values) represents the results from the training of the LSTM model. The red line (test predictive values) represents the SPEI values predicted by the model for 2020 from those between 1980 and 2019.

Figure 3 shows that the training results of the LSTM model basically agreed with the SPEI values calculated based on weather station observations. The two had a similar variation trend, indicating that the LSTM model correctly simulated the variation in SPEI values. Besides, the LSTM model also predicted a sudden decrease between 2009 and 2010 which southwest China encountered extreme drought once in a century, demonstrating the reliability of the training results. However, we also found that the training results were smaller than SPEI values calculated based on weather station observations, and the former changed less significantly. This was probably because the model had a worse learning ability for samples with a smaller proportion (such as severe drought and extreme drought), but a stronger ability in learning the overall trend. Generally speaking, the model-predicted variation trend of SPEI values for 2020 was similar to the variation in SPEI values calculated based on weather station observations.

3.2 LSTM model accuracy evaluation

We first compared the SPEI values calculated based on weather station observations against the actual drought statistics for 2020 [66] before comparing the LSTM-predicted SPEI values against the SPEI values calculated based on weather station observations to improve the model prediction accuracy. In this way, we determined whether the SPEI values calculated based on weather station observations correctly reflected the actual spatial distribution of drought in southwest China in 2020. Table 3 shows the actual drought situation in southwest China in 2020. Figure 4 shows the results of spatial monitoring of droughts based on a monthly-scale SPEI following drought grade classification in Table 1 and by performing spatial interpolation using SPEI values calculated based on 144 weather station observations in southwest China in 2020.

Figure 4 shows that drought was infrequent in the entire southwest China in January and February. However, a severe drought hit Yunnan, Sichuan, and eastern Tibet in March. The entire Yunnan was struck by a drought of moderate severity and above. Severe and extreme drought affected southwestern Sichuan, while mild and moderate drought occurred in eastern Tibet. The drought was

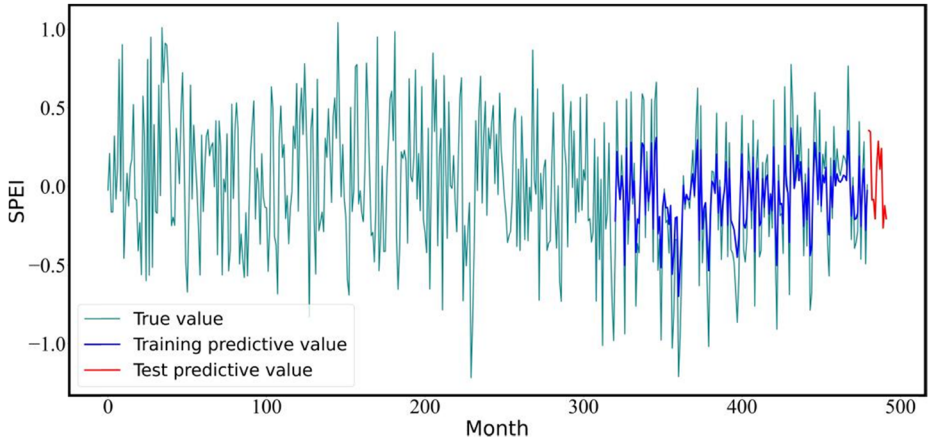

Figure 3: Average time changes of SPEI on calculating values based on 144 weather stations from 1980 to 2019, training values from 1980 to 2019, and predictive values in 2020 based on the LSTM model.

Table 3: Actual drought conditions in 2020 in southwest China

Region	Sichuan	Yunnan	Guizhou	Chongqing	Tibet
Drought situation	Fast worsening drought in May and June, with drought relieved from the second 10 day period of June to early July	Drought occurring in most regions of the central part, southern region of the northwestern part, and western region of the southeastern part from January to June; severe drought, particularly in spring in the central and southern parts, reaching the peak at the end of May; gradually increasing precipitation in July, with drought gradually relieved in the western part; the drought persisting into the first 10 day period of August in the central and eastern parts; severe winter drought at the end of the year	Fast worsening drought from early May to the second 10 day period of June, with drought relieved from the second 10 day period of June to early July	Fast worsening drought in May and June, with drought relieved from the second 10 day period of June to early July	Little precipitation in Ngari Prefecture in the western part since July, with drought of moderate severity and above in some regions; severe drought in Shiquanhe Town and Purang County; severe drought in the western and central parts of Tibet from September to October

relieved in southwest China in April, but worsened in Yunnan in May and June. Moderate-to-severe drought occurred in southern Yunnan, and moderate drought in Sichuan and Chongqing. The drought was lessened in the Sichuan–Chongqing region in June. The drought appeared in western Tibet in July and worsened over time. Most parts of Tibet were inflicted by extreme drought in October, and the drought severity peaked in this month. The drought was relieved in November and December. From July to October, the drought was also relieved in Yunnan, Guizhou, Sichuan, and Chongqing. A drought of moderate severity and above hit extensive regions of Yunnan, Sichuan, Guizhou, and Chongqing in November. The drought disappeared in Guizhou and Chongqing in December, while severe drought hit southern Yunnan and western Sichuan. As shown by actual drought statistics in Table 3, drought mainly occurred in Yunnan as far as southwest China was concerned. The spring drought was particularly severe and extensive in Yunnan, reaching its peak at the end of May. The drought was gradually relieved by rainfalls in June and July, although it persisted into August in central and eastern Yunnan. Severe drought recurred in Yunnan at the end of 2020. In Sichuan, Guizhou, and Chongqing, drought mainly occurred in May and June and was basically relieved in July. Starting from July, western Tibet was hit by a drought of moderate severity and above. Drought was severe in western and central Tibet in September and October. A combined analysis of Figure 4 and Table 3 shows that the monthly drought-grade monitoring based on SPEI values calculated from weather station observations generally agreed with the spatial distribution of the actual drought situation. This indicated that SPEI enabled effective and correct monitoring of drought grades and distribution in southwest China. Therefore, we could reliably compare the SPEI values calculated from weather station observations against the drought monitoring results from the LSTM model to assess model accuracy.

In this study, five indicators, namely, R^2, RMSE, EVS, NSE, and KGE, were chosen as the accuracy assessment indicators of the LSTM model. The values of these five indicators are listed in Table 4.

Table 4 demonstrates that when two-thirds of the samples from 1980 to 2019 were used as the training set and the remaining one-third as the test set, the model yielded more favorable training results. The R^2 value for the predicted SPEI on the test set, compared to the 1 month scale SPEI (SPEI-1) calculated from weather station observations, was 0.757, indicating a significant correlation. Additionally, the RMSE and EVS on the test set were 0.210 and 0.802, respectively. The small RMSE and EVS values close to 1 indicate high prediction accuracy and strong agreement with actual observations. The NSE was 0.761, falling within the range of

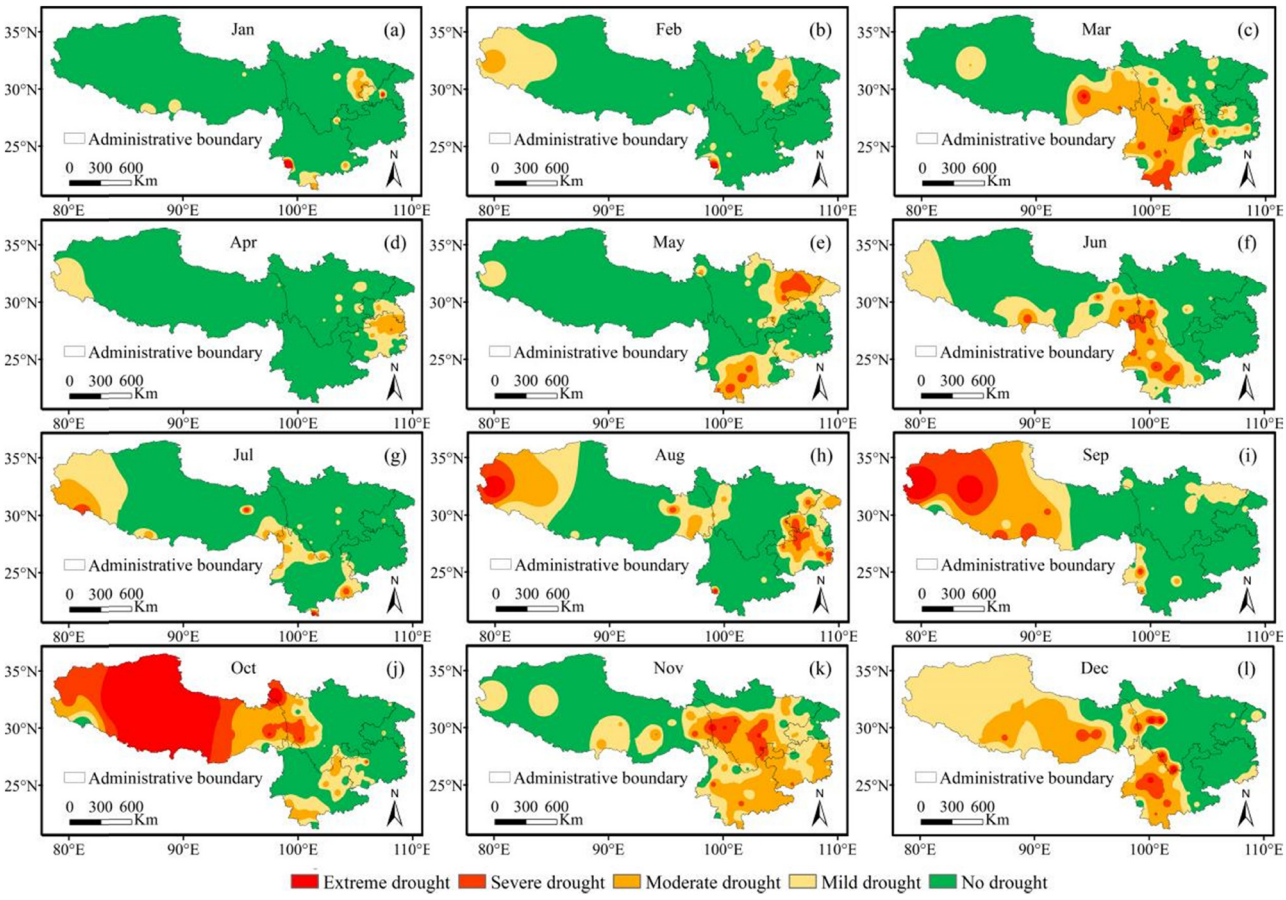

Figure 4: Monthly-scale SPEI-based drought monitoring in southwest China for 2020. (a) Jan. (b) Feb. (c) Mar. (d) Apr. (e) May (f) Jun. (g) Jul. (h) Aug. (i) Sep. (j) Oct. (k) Nov. (l) Dec.

0.7 to 0.9, which signifies great prediction success. The KGE was 0.212, a value greater than 0 and less than 1, suggesting a certain level of reliability in the model predictions. Overall, the model exhibited a good prediction performance. The training results of the LSTM model on the training set shared a similar variation trend as the actual observations, thus indicating that the model predictions were generally reliable.

Table 4: Predictive accuracy evaluation results of the LSTM model

Accuracy assessment indicators	Value
R^2	0.757
RMSE	0.210
EVS	0.802
NSE	0.761
KGE	0.212
Total consistency rate of drought grade	59.26%

3.3 RF benchmark model construction and comparative analysis

An RF benchmark model was constructed using the same data and dataset partitioning method. Table 5 details the optimal parameters for the final RF prediction model. Table 6 provides the accuracy evaluation results using the five metrics: R^2, RMSE, EVS, NSE, and KGE.

Comparing the results presented in Table 6 with those in Table 4, it was observed that in the test set, the accuracy evaluation indices were as follows: $0 < R^2 < 0.757$, $0 <$ RMSE and $0.210 <$ RMSE, $0 <$ EVS < 0.802, NSE < 0 and NSE < 0.761, $0 <$ KGE < 0.212. The RF model demonstrated relatively poor performance overall, whereas the LSTM model exhibited superior evaluation performance compared to the RF model. This discrepancy is considered to be potentially related to the smaller number of features selected and the shorter time scale of the time series studied. Given that drought events inherently involve temporal dependencies and that LSTM model is better suited for handling

Table 5: Optimal parameters of the RF prediction model

Parameters	Description	Optimal value
Max_features	Maximum features per decision tree	"auto"
Bootstrap	Whether sampling is performed with or without replacement	True
Criterion	Criteria for evaluating split quality	mse
Max_depth	Tree depth limit	2
Min_samples_split	Minimum samples for node splitting	2
Min_samples_leaf	Minimum samples per leaf node	3
n_Estimators	Total number of decision trees	69

Table 6: Predictive accuracy evaluation results of the RF model

Accuracy assessment indicators	Value
R^2	0.350
RMSE	0.409
EVS	0.017
NSE	−0.036
KGE	0.044
Total consistency rate of drought grade	40.10%

time-series data with long-term dependencies, the prediction performance of LSTM is relatively better.

3.4 LSTM model comparison and validation

The consistency rate of each drought grade was estimated based on LSTM-predicted SPEI-1 for 2020 and the SPEI-1 values calculated from weather station observations for 2020. However, the consistency rates of drought grades are affected by the total sample size, distribution of different drought grades at each weather station, and the one-to-one single feature prediction. Our analysis showed that the total consistency rate of drought grade was high, the value being 59.26% (Table 4). Specifically, the consistency rate was highest for no drought, which was 75.68%. The consistency rate was more than 50% for mild and moderate drought, and it was 42.56% for severe drought. It was the lowest for extreme drought, which was only 24.32%. In comparison, the RF model achieved a lower overall consistency rate of 40.10% (Table 6), further highlighting the superior predictive reliability of the LSTM model.

Figure 5 shows the scatter plots of the SPEI-1 values predicted by the LSTM and RF models compared to those calculated by meteorological stations for the year 2020.

The scatter plot in Figure 5 showed that the prediction accuracy of both models for 2020 was suboptimal, with the SPEI index displaying a comparatively narrow value range. However, the LSTM model outperformed the RF model significantly in terms of prediction accuracy. The underlying reasons can be analyzed as follows: first, the calculation was based not on the SPEI-1 values from a single meteorological station, but on the averaged SPEI-1 values across 144 meteorological stations in southwest China, resulting in a more compressed value range. Second, the

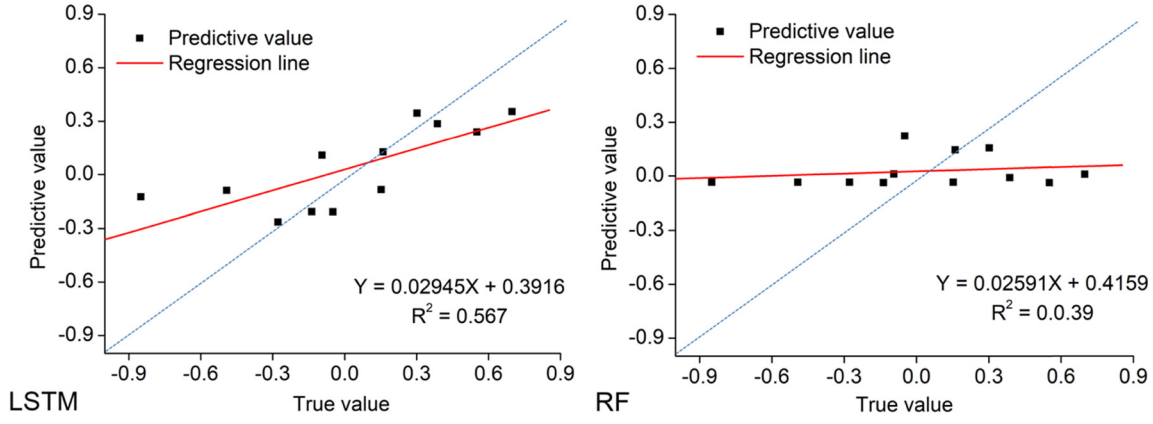

Figure 5: Scatter plots of SPEI-1 values predicted by the LSTM and RF models compared to the true values for 2020.

data used comprised single-feature SPEI-1 sample data derived from these 144 stations from 1980 to 2019. The limited number of samples, coupled with the selected feature variable, reduced the predictive robustness, particularly given the scarcity of learning samples representing extreme and severe droughts over this 40 year span. In 2020, some regions and seasons in the southwest China experienced extreme drought and severe drought events, which considerably impacted the models' predictions, shifting the predicted value range toward the more frequent no drought and mild drought cases. Finally, the 2020 prediction was based on only 12 months of data, which limited the models' learning potential and leaded to less pronounced results. However, due to the LSTM model's ability to retain long-term information through its memory units and capture temporal dependencies across extended sequences, it is better suited to predicting long-term patterns, explaining its superior performance compared to the RF model.

Additionally, a Kruskal–Wallis test was performed to statistically compare the predicted values with the observed values. The Kruskal–Wallis test is a non-parametric method used to assess whether two or more samples originate from the same probability distribution. The results of this test for both models are presented in Table 7. As illustrated in the table, the H_0 hypothesis was rejected for the predictions of both models using the SPEI-1 data. This result indicates that there was no significant difference between the distributions of the predicted and observed data.

Figure 6 shows the temporal variations in the SPEI values calculated from weather station observations in southwest China for 2020 and those in SPEI values predicted using the LSTM model for 2020.

Figure 6 presents that the LSTM-predicted SPEI values for 2020 shared a similar variation trend with the SPEI values calculated from weather station observations. A decreasing trend was observed for both, indicating an arid trend in southwest China in 2020. Except for November, the monthly variation trends of SPEI values were basically the same, but the specific SPEI values differed significantly.

Table 7: *P*-values of Kruskal–Wallis test at 95% significance level

Models	SPEI-1	
	***p* value**	***H_0**
LSTM	0.862	Reject
RF	0.967	Reject

H_0: There are differences between mean predicted and measurement values.
* indicates passing the significance level test of 0.05.

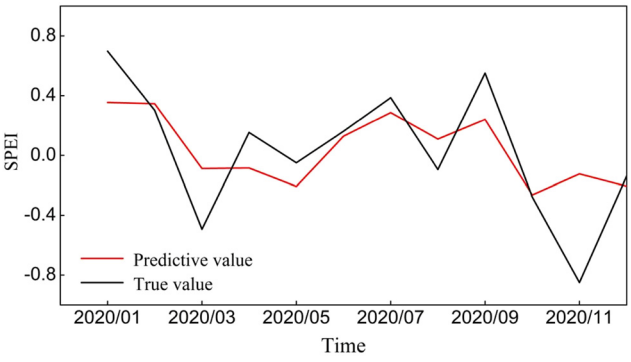

Figure 6: Average temporal changes in SPEI values between LSTM model prediction and calculation based on 144 meteorological stations in 2020.

The model predictions revealed smaller SPEI values but more steady variations. According to the drought-grade classification based on SPEI values in Table 1, the drought grades were normal in all 12 months. However, a milder drought was indicated for November due to significant intermonthly variations in SPEI values calculated from weather station observations. A larger difference between the results of the two methods might be due to the accumulation of errors as the prediction proceeded. Besides, a milder change in SPEI values for the prior time step might affect the predicted value of the next time step. Nevertheless, the variation trends obtained by the two methods were similar to those in Figure 3. That is to say, the LSTM model could reflect the future variation trend of drought in southwest China to a certain degree and therefore had certain reliability. Figure 7 shows the results of spatial interpolation of the correlation between the two.

Figure 7 shows that the CCs were above 0.5 for most regions. The degree of correlation was higher in Tibet and Sichuan. Particularly, the CCs exceeded 0.6 in western Tibet and Chengdu Plain. However, the degree of correlation was lower in the junction between Chongqing and

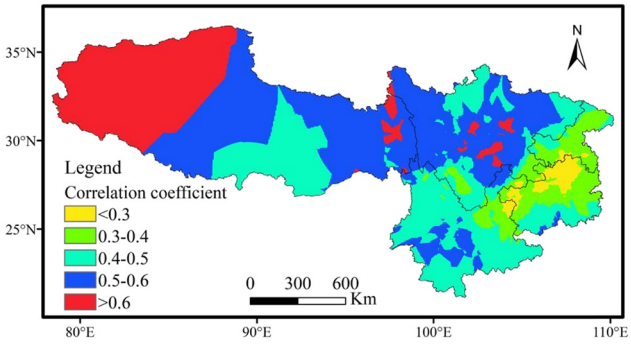

Figure 7: Spatial correlation distribution of SPEI-1 values between LSTM model prediction and calculation based on meteorological stations in 2020.

Guizhou, and the CCs were below 0.4. This was probably because the junction between Guizhou and Chongqing was dominated by hilly terrain, resulting in smaller variations in the SPEI-1 values and lower prediction accuracy. The CCs were generally above 0.4 in Yunnan. The significance test for the correlation between the results of the two methods indicated a significant correlation at more than one half of 144 weather stations. The aforementioned results demonstrated the reliability and applicability of the LSTM model in SPEI predictions. However, the degree of correlation and the significance level between the results of the two methods might be strongly related to the number and spatial distribution of weather stations in the study area.

4 Discussion

Conducting a series of studies on drought monitoring, assessment, and prediction has become a hot issue of immense global concern and is of great practical significance [6]. ML is a powerful and widely used technique for prediction models. However, on the condition of Big Data, DL is considered a better solution. Currently, data-driven models represented by DL are also being widely used in time-series prediction and simulation of drought [43].

From 1980 to 2019, the R^2 value of the predicted SPEI using the LSTM model on the test set relative to SPEI calculated from weather station observations was 0.757, indicating a significant correlation. RMSE was small, EVS was close to 1, the value of NSE ranged between 0.7 and 0.9, and KGE was close to 0, with values being 0.210, 0.802, 0.761, and 0.212, respectively. The Kruskal–Wallis test revealed no significant difference in the distributions between the predicted and observed data. The predicted SPEI values for 2020 basically coincided with the SPEI values calculated from weather station observations. Except for November, the variation trends of SPEI for other months were basically consistent using the two methods. The scatter plot of the LSTM model for 2020 was clearly superior to that of the benchmark RF model. The spatial CCs for most regions were high and more than 0.5 for the two methods, but lower in other regions (less than 0.3). The total consistency rate for all drought grades was not very high, the value being 59.26%. Particularly, the consistency rate was low for severe drought (42.56%) and extreme drought (24.32%), which might be explained by the following reasons: (1) the samples available for learning were few. In the present study, the monthly SPEI values in 40 years from 1980 to 2019 were used, and approximately 480 samples were evaluated. Severe and extreme drought events were very rare during this period, leading to inadequate learning of severe and extreme drought; (2) few learning elements were present as model inputs. One-to-one time-series prediction was performed during the learning process. In this study, we only performed a simulated prediction based on monthly SPEI values from 1980 to 2019 without considering other influencing factors. For this reason, the learning ability and accuracy of the model were affected to some degree. Besides, during one-to-one cyclic time-series prediction, the longer the prediction time, the lower the prediction accuracy due to the inherent problems of the model. This fact gave rise to randomness and uncertainty; (3) errors accumulated during model predictions. A milder change in SPEI values for the prior time step might affect the predicted value for the next time step; and (4) the number and spatial distribution of weather stations within the study area and the distribution of different drought grades at each weather station also impacted errors. Comprehensively speaking, the LSTM model constructed in this study had a high prediction accuracy, and the predicted values were close to actual observations. The predicted values somewhat reflected the future variation trend of drought in southwest China.

In addition, the data of SPEI with a 1 month timescale changed relatively fast and fluctuated more. Hence, the predicted values of LSTM for the 114 meteorological stations were different from the true SPEI values on the 1 month timescale, which was also consistent with the conclusion reached by Xu et al. [67]. When the timescale increased, the data series tended to be smooth and the prediction accuracy of the LSTM model gradually improved [6]. This study only discussed meteorological drought for 1 month scale SPEI. Therefore, the drought prediction results of the LSTM model on more timescales require further analysis, comparison, and discussion.

Compared to other similar studies, this study has the following features: (1) DL methods are currently seldom used for drought prediction in southwest China, making our study a significant contribution for similar regions; (2) while most studies using ML for drought prediction focus on one or a few weather stations, our research uses data from 144 weather stations. We performed a comprehensive average analysis and assessed the consistency of drought predictions across different intensity levels at all stations; and (3) in evaluating the LSTM model, we not only calculated five performance metrics but also analyzed scatter plots, conducted the Kruskal–Wallis test, compared results with a benchmark RF model, performed correlation analysis, and compared predictions with actual drought events. This approach makes our study more thorough and comprehensive than others.

5 Conclusions

Accurate prediction of drought can effectively reduce the risk of drought. However, drought is difficult to predict and is considered one of the severest natural disasters. Particularly, drought prediction can be highly challenging in regions with complex terrain, topography, and formative factors of weather and climate and where weather stations are sparsely distributed. However, the data-driven DL method can be used to mine drought features from different perspectives and can improve the generalization ability and accuracy of drought prediction. The present study focused on southwest China where drought disasters occur frequently and at high intensity. The LSTM predictive model was constructed by calculating SPEI values based on 144 weather station observations from 1980 to 2020. The performance of the model was comprehensively assessed and validated in various ways. The conclusions of the study were as follows.

(1) The training results of the LSTM model basically agreed with the SPEI values calculated based on weather station observations. The LSTM model also predicted a sudden decrease between 2009 and 2010 which southwest China encountered extreme drought once in a century. The model-predicted variation trend of SPEI values for 2020 was similar to the variation in SPEI values calculated from weather station observations.
(2) Monthly drought-grade monitoring based on SPEI values calculated from weather station observations generally agreed with the spatial distribution of the actual drought situation in 2020. This indicated that we could reliably compare the SPEI values calculated from weather station observations against the drought predicting results from the LSTM model to assess model accuracy.
(3) The R^2 value of the predicted SPEI by LSTM model on the test set relative to the SPEI calculated from weather station observations was 0.757. The values of RMSE, EVS, NSE, and KGE were 0.210, 0.802, 0.761, and 0.212, respectively. The total consistency rate of drought grade was 59.26%. Furthermore, the Kruskal–Wallis test confirmed that there were no significant differences between the distributions of the predicted and observed data. The LSTM model predictions were generally reliable.
(4) Compared to the benchmark RF model, the LSTM model excelled in all five performance evaluation metrics and demonstrated a higher overall consistency rate for drought categories. The Kruskal–Wallis test for the RF model also indicated no significant difference in the distributions between the predicted and observed data. Scatter plots revealed that the prediction accuracy of both the LSTM and RF models for 2020 was suboptimal, with the SPEI showing a comparatively narrow range of values. Nonetheless, the LSTM model significantly outperformed the RF model in terms of prediction accuracy, providing more accurate and reliable drought predictions.
(5) The spatial correlation distribution of SPEI values between LSTM model prediction and calculation based on meteorological stations in 2020 was above 0.5 for most regions. The CCs exceeded 0.6 in western Tibet and Chengdu Plains.

The LSTM model demonstrated a significant improvement in drought prediction performance compared to the benchmark RF model. However, to reduce model complexity and enhance computational efficiency, this study used only a single feature for drought prediction and employed data with a time span of only 20 years. This limited sample size and number of features may impact prediction accuracy. Therefore, based on the analysis and discussion above, it is recommended to adopt the following approaches to further improve drought prediction in southwest China and enhance the model's accuracy, robustness, and generalization capability. Increasing the number of samples and incorporating additional variables related to drought causes into the LSTM model could be beneficial. Utilizing the food and agriculture organization-united nations Penman–Monteith method for estimating PET can provide more accurate calculations of the SPEI. Additionally, integrating or hybridizing the LSTM model with other statistical models, traditional ML models, and DL models could leverage the strengths of various approaches, mitigate potential biases, and improve overall prediction accuracy [68].

Acknowledgement: This work was jointly funded by the Key Research and Development (R&D) Project in Department of Science and Technology of Yunnan Province (202203AC100005, 202203AC100006), Open Project of the Research Center for Meteorological Disaster Prediction, Early Warning and Emergency Management at the Key Research Base of Humanities and Social Sciences of the Sichuan Provincial Department of Education (ZHYJ23-ZD01), and the Drought Meteorological Science Research Fund of the China Meteorological Administration (IAM202201).

Author contributions: Project suggested by WL and XTG. Analysis done by LXH and JHJ. Data and comments contributed by LXH and JHJ. Article written by LXH, JHJ, WL, and XTG. All authors revised it critically for important intellectual content.

Conflict of interest: The authors state no conflict of interest.

References

[1] Zhang X, Hao ZC, Singh VP, Zhang Y, Feng SF, Xu Y. Drought propagation under global warming: Characteristics, approaches, processes, and controlling factors. Sci Total Environ. 2022;838:156021.

[2] Dikshit A, Pradhan B, Santosh M. Artificial neural networks in drought prediction in the 21st century-A scientometric analysis. Appl Soft Comput. 2022;114:108080.

[3] Danandeh MA, Rikhtehgar GA, Yaseen ZM, Unal SA, Abualigah L. A novel intelligent deep learning predictive model for meteorological drought forecasting. J Ambient Intell Humanized Comput. 2023;14:10441–55.

[4] United Nations Convention to Combat Desertification (UNCCD). Drought in Numbers 2022, the 15th Session of the Conference of the Parties to the UNCCD. New York, USA: United Nations; 2022. https://www.unccd.int/sites/default/files/2022-05/Drought_in_Numbers_%28English%29.pdf.

[5] Liu M, Zai G, Wang G, Shi W, Zhang G. Research on the application of artificial intelligence algorithms in drought prediction. Proceedings of the 2022 6th International Conference on Electronic Information Technology and Computer Engineering; 2022. p. 1845–50.

[6] Shang J, Zhao B, Hua H, Wei J, Qin G, Chen G. Application of informer model based on SPEI for drought forecasting. Atmosphere. 2023;14:951.

[7] Firdaus T, Gupta P, Sangita MS. Implementing machine learning models for drought prediction based on metrological drought indices with varying time scales: A case of Latur Region. Recent Advances in Sustainable Environment: Select Proceedings of RAISE 2022. Singapore: Springer Nature Singapore; 2022. p. 183–95.

[8] Ding Y, Yu G, Tian R, Sun Y. Application of a hybrid CEEMD-LSTM model based on the standardized precipitation index for Drought forecasting: The case of the Xinjiang Uygur Autonomous Region, China. Atmosphere. 2022;13:1504.

[9] Ma X, Yao Y, Zhao Q. Regional GNSS-Derived SPCI: Verification and improvement in Yunnan, China. Remote Sens. 2021;13:1918.

[10] Das J, Jha S, Goyal MK. Non-stationary and copula-based approach to assess the drought characteristics encompassing climate indices over the Himalayan states in India. J Hydrol. 2020;580:124356.

[11] Rezaeianzadeh M, Stein A, Cox JP. Drought forecasting using Markov chain model and artificial neural networks. Water Resour Manag. 2016;30:2245–59.

[12] Balti H, Abbes AB, Mellouli N, Imed RF, Sang YF, Lamolle M. A review of drought monitoring with big data: Issues, methods, challenges and research directions. Ecol Inf. 2020;60:101136.

[13] Jiao W, Wang L, Mccabe MF. Multi-sensor remote sensing for drought characterization: Current status, opportunities and a roadmap for the future. Remote Sens Environ. 2021;256:112313.

[14] Park S, Im J, Jang E, Rhee J. Drought assessment and monitoring through blending of multi-sensor indices using machine learning approaches for different climate regions. Agric Meteorol. 2016;216:157–69.

[15] Cao J, Zhang Z, Tao F, Zhang L, Luo Y, Zhang J. Integrating multi-source data for rice yield prediction across China using machine learning and deep learning approaches. Agric For Meteorol. 2021;297:108275.

[16] Kafy AA, Bakshi A, Saha M, Faisal AA, Almulhim AL, Rahaman ZA, et al. Assessment and prediction of index based agricultural drought vulnerability using machine learning algorithms. Sci Total Environ. 2023;867:161394.

[17] Agana NA, Homaifar A. A deep learning based approach for long-term drought prediction. SoutheastCon 2017. IEEE. 2017;1–8.

[18] Liu ZN, Li QF, Nguyen LB, Xu GH. Comparing machine-learning models for drought forecasting in Vietnam's Cai River Basin. Pol J Environ Stud. 2018;27:2633–46.

[19] Jiang W, Luo J. An evaluation of machine learning and deep learning models for drought prediction using weather data. J Intell Fuzzy Syst. 2022;43:3611–26.

[20] Mokhtar A, Jalali M, He H, Al-Ansari N, Elbeltagi A, Alsafadi K, et al. Estimation of SPEI meteorological drought using machine learning algorithms. IEEE Access. 2021;9:65503–23.

[21] Alawsi MA, Zubaidi SL, Al-Bdairi NSS, Ai-Ansari N, Hashim K. Drought forecasting: A review and assessment of the hybrid techniques and data pre-processing. Hydrology. 2022;9:115.

[22] Achite M, Jehanzaib M, Elshaboury N, Kim TW. Evaluation of machine learning techniques for hydrological drought modeling: A case study of the Wadi Ouahrane basin in Algeria. Water. 2022;14:431.

[23] Hinton GE, Salakhutdinov RR. Reducing the dimensionality of data with neural networks. Science. 2006;313:504–7.

[24] Kaur A, Sood SK. Deep learning based drought assessment and prediction framework. Ecol Inform. 2020;57:101067.

[25] Prodhan FA, Zhang JH, Yao FM, Shi LM, Pangali STP, Zhang D, et al. Deep learning for monitoring agricultural drought in South Asia using remote sensing data. Remote Sens. 2021;13:1715.

[26] Docheshmeh GA, Alizamir M, Kisi O, Elshafie A. Drought modelling by standard precipitation index (SPI) in a semi-arid climate using deep learning method: Long short-term memory. Neural Comput Appl. 2022;34:2425–42.

[27] Poornima S, Pushpalatha M. Drought prediction based on SPI and SPEI with varying timescales using LSTM recurrent neural network. Soft Comput. 2019;23:8399–412.

[28] Docheshmeh GA, Alizamir M, Kisi O, Elshafie A. Drought modelling by standard precipitation index (SPI) in a semi-arid climate using deep learning method: long short-term memory. Neural Comput and Appl. 2022;34:2425–42.

[29] Dikshit A, Pradhan B, Huete A. An improved SPEI drought forecasting approach using the long short-term memory neural network. J Environ Manag. 2021;283:111979.

[30] Wang T, Tu X, Singh VP, Chen XH, Lin KR, Zhou ZL. Drought prediction: Insights from the fusion of LSTM and multi-source factors. Sci Total Environ. 2023;902:166361.

[31] Villegas-Ch W, García-Ortiz J. A long short-term memory-based prototype model for drought prediction. Electronics. 2023;12(18):3956.

[32] Li X, Jia H, Wang L. Remote sensing monitoring of drought in Southwest China using random forest and extreme gradient boosting methods. Remote Sens. 2023;15:4840.

[33] Zhang Q, Yao YB, Li YH, Huang JP, Ma ZG, Wang ZL, et al. Progress and prospect on the study of causes and variation regularity of droughts in China. Acta Meteorologica Sin. 2020;78:500–21.

[34] Wang YS, Xiao TG, Dong XF. Characteristics of long-cycle abrupt drought-flood alternations in Southwest China and atmospheric circulation in summer from 1961 to 2019. Plateau Meteorol. 2021;40:760–72.

[35] Huan DB, Fan K, Xu ZQ. Strengthened relationship between summer Barents sea ice and autumn Southwest China drought after the mid-and late-1990s. Trans Atmos Sci. 2022;45:167–78.

[36] Hatami BBP, Luo LF, Tan PN, Pei LS. Automated analysis of the US drought monitor maps with machine learning and multiple drought indicators. Front Big Data. 2021;4:750536.

[37] Zhang ZB, Yang Y, Zhang XP, Chen ZJ. Wind speed changes and its influencing factors in southwestern China. Acta Ecologica Sin. 2014;34:471–81.
[38] Zhang Q, Li YQ. Climatic variation of rainfall and rain day in Southwest China for last 48 years. Plateau Meteorol. 2014;33:372–83.
[39] Li Q, Wang XM, Zhou GB, Zhang YP, He Y. Temporal and spatial distribution characteristics of short-time heavy rainfall during southwest vortex rainstorm in Sichuan Basin. Plateau Meteorol. 2020;39:960–72.
[40] Li XH, Chen ZF, Wang L. Analysis of the spatiotemporal variation characteristics of main extreme climate indices in Sichuan Province of China from 1968 to 2017. Appl Ecol Environ Res. 2020;18(2):3211–42.
[41] China Meteorological Administration. China Climate Bulletin. Beijing, China: China Meteorological Administration; 2020. p. 1–56. https://www.cma.gov.cn/zfxxgk/gknr/qxbg/202104/t20210406_3051288.html.
[42] Vicente-Serrano SM, Beguería S, López-Moreno JIJJ. A multiscalar drought index sensitive to global warming: The standardized precipitation evapotranspiration index. J Clim. 2010;23:1696–718.
[43] Li XH, Jia HJ, Meng C, Liu HS, Xia YY. Evaluation of the applicability of multiple remote sensing drought indices for monitoring of dry and wet in southwest China. Second International Conference on Geographic Information and Remote Sensing Technology (GIRST 2023). Qingdao, China: SPIE; Vol. 2797, 2023. p. 540–8.
[44] National Standard of the People's Republic of China. Meteorological Drought Level. Standardization Administration of China (GB/T 20481-2017). 2018.
[45] Rhee J, Im J. Meteorological drought forecasting for ungauged areas based on machine learning: Using long-range climate forecast and remote sensing data. Agric For Meteorol. 2017;237:105–22.
[46] Wang Q, Zeng J, Qi J, Zhang X, Zeng Y, Shui W, et al. A multi-scale daily SPEI dataset for drought characterization at observation stations over mainland China from 1961 to 2018. Earth Syst Sci Data. 2021;13(2):331–41.
[47] Pyarali K, Peng J, Disse M, Tuo Y. Development and application of high resolution SPEI drought dataset for Central Asia. Sci Data. 2022;9(1):172.
[48] Dukat P, Bednorz E, Ziemblińska K, Urbaniak M. Trends in drought occurrence and severity at mid-latitude European stations (1951-2015) estimated using standardized precipitation (SPI) and precipitation and evapotranspiration (SPEI) indices. Meteorol Atmos Phys. 2022;134(1):20.
[49] Hochreiter S, Schmidhuber J. Long short-term memory. Neural Comput. 1997;9(8):1735–80.
[50] Yin Z, Qin G, Guo L, Tang X, Wang J, Li H. Coupling antecedent rainfall for improving the performance of rainfall thresholds for suspended sediment simulation of semiarid catchments. Sci Rep. 2022;12:4816.
[51] Gers FA, Schmidhuber J, Cummins F. Learning to forget: Continual prediction with LSTM. Neural Comput. 2000;12:2451–71.
[52] Vo TQ, Kim SH, Nguyen DH, Bae DH. LSTM-CM: A hybrid approach for natural drought prediction based on deep learning and climate models. Stoch Environ Res Risk Assess. 2023;37(6):2035–51.
[53] Breiman L. Random forests. Mach Learn. 2001;45:5–32.
[54] Xie L, Meng X, Zhao X, Fu L, Sharma RP, Sun H. Estimating fractional vegetation cover changes in desert regions using RGB data. Remote Sens. 2022;14(15):3833.
[55] Uncuoglu E, Citakoglu H, Latifoglu L, Bayram S, Laman M, Ilkentapar M, et al. Comparison of neural network, Gaussian regression, support vector machine, long short-term memory, multi-gene genetic programming, and M5 Trees methods for solving civil engineering problems. Appl Soft Comput. 2022;129:109623.
[56] Kling H, Fuchs M, Paulin M. Runoff conditions in the upper Danube basin under an ensemble of climate change scenarios. J Hydrol. 2012;424:264–77.
[57] Nash JE, Sutcliffe JV. River flow forecasting through conceptual models part I-A discussion of principles. J Hydrol. 1970;10(3):282–90.
[58] Citakoglu H. Comparison of multiple learning artificial intelligence models for estimation of long-term monthly temperatures in Turkey. Arab J Geosci. 2021;14(20):2131.
[59] Citakoglu H, Coşkun Ö. Comparison of hybrid machine learning methods for the prediction of short-term meteorological droughts of Sakarya Meteorological Station in Turkey. Environ Sci Pollut Res. 2022;29(50):75487–511.
[60] Guo X, Yu HB, Ma ZC, Cao CM. Analysis of spatial and temporal variations of soil moisture content and drought degree based on MODIS. Resour Soil Water Conserv. 2019;26:185–9+2.
[61] Park S, Im J, Park S, Rhee J. Drought monitoring using high resolution soil moisture through multi-sensor satellite data fusion over the Korean Peninsula. Agric For Meteorol. 2017;237:257–69.
[62] Shen RP, Guo J, Zhang JX, Li LX. Construction of a drought monitoring model using the random forest based on remote sensing. J Geo-information Sci. 2017;19:125–33.
[63] Deng JH. Deep learning – principles, models and practice. Beijing: Posts Telecom Press; 2021. p. 47–50.
[64] Jia HJ. Construction and application of remote sensing drought monitoring model based on machine learning in Southwestern China. Chengdu, China: Chengdu University of Information Technology; 2022.
[65] Dai TL, Wang QL, Wang GF, Chen Y, Zhao SS, Zhai JQ, et al. Climatic characteristics major meteorological events over China in 2020. Meteor Mon. 2021;47:478–87.
[66] Yan D, Jiang R, Xie J, Zhao Y, Zhu J, Liang J. Characteristics and prediction of extreme drought event using LSTM model in Wei River Basin. Terrestrial Atmos Ocean Sci. 2021;32(2):261–74.
[67] Xu D, Ding Y, Liu H, Zhang Q, Zhang D. Applicability of a CEEMD-ARIMA combined model for drought forecasting: A case study in the Ningxia Hui Autonomous Region. Atmosphere. 2022;13:1109.
[68] Li S, Xie J, Yang X, Jing X Comparison of hybrid machine learning models to predict short-term meteorological drought in Guanzhong Region, China. Water Sci Technol. 2023;87(11):2756–75.